Phytosynthesis of silver nanoparticles; naked eye cellulose filter paper dual mechanism sensor for mercury ions and ammonia in aqueous solution

Muhammad Ismail[1] · M. I. Khan[1] · Kalsoom Akhtar[2] · Jongchul Seo[3] · Murad Ali Khan[1] · Abdullah M. Asiri[2,4] · Sher Bahadar Khan[2,4]

Abstract

In the present study, low cost novel cellulose filter paper based silver nanoparticles (CF-AgNPs) sensor was developed. AgNPs were synthesized via green approach using aqueous leaf extract of *Convolvulus cneorum* (*C. cneorum*). The prepared AgNPs were characterized by UV–visible spectroscopy, powder X-ray diffraction (XRD), field emission scanning electronic microscopy (FE-SEM) and energy dispersive X-ray spectroscopy (EDX). Fourier-transform infrared spectroscopy (FTIR) study revealed the role of *C. cneorum* metabolites in the reduction of Ag^+ ions into AgNPs and their stabilization. Fast, low cost, single step and selective detection of carcinogenic heavy metals in the environmental sample is significant to take safety action. Prepared AgNPs showed a potential colorimetric detection limit for toxic mercury Hg^{II} around 5 ppb and Cr^{VI} up to 5 ppm. Addition of Hg^{II}, Cr^{VI} and ammonia showed marked blue shift in the surface plasmon resonance (SPR) peak of AgNPs. Of importance, this AgNPs probe was not only successfully applied for the detection of Hg^{II}, but also it could be used in the sensing of Cr^{VI} and aqueous ammonia. Thus, due to the distinctive localized SPR, high sensitivity, simplicity, lower detection limit at ppb level and rapid response time are the most useful for the colorimetric detection of aqueous ammonia and Hg^{II} at room temperature.

1 Introduction

Nanotechnology is the novel field of science and technology presenting materials having structural characteristics between those of bulk and atoms size [1]. Nanotechnology is the emerging interdisciplinary field of science and technology that link material science and life science [2]. Nanomaterials are the structured components in which one of its dimensions (width, length or thickness) is at least in size range from 1 to 100 nm [3]. Research on nanoparticles, especially metal nanoparticles have increased extensively due to their remarkable physical, mechanical, optical, chemical, magnetic and electrical properties [4]. Different methods have been used for the synthesis of nanoparticles, including biological, physical and chemical syntheses. Physical and chemical methods are cumbersome and expensive, while green synthesis method is cost efficient and environment friendly compared to conventional chemical and physical methods. In plant mediated synthesis, the aqueous plant extract is used which contain phytochemicals. These phytochemicals are responsible for the reduction as well as stabilization of nanoparticles. This makes them more advantageous over physical and chemical synthesis methods [5]. Plants such as melon [6], *Durenta erecta* [7], *Gymnema sylvestre, Scilla peruvina, Rubia cordifolia* [8], *Areca catechu* [9], *Lawsonia inermis* [10], *Cydonia oblong* [11] have been used currently for the synthesis of silver nanoparticles. Among the various metals; silver is one of the most important metal because it is used as an antimicrobial agent and help in protection against the increasing risk caused by antibiotic resistant bacteria [12].

✉ Sher Bahadar Khan
sbkhan@kau.edu.sa

1 Department of Chemistry, Kohat University of Science & Technology, Kohat 26000, Khyber Pakhtunkhwa, Pakistan

2 Chemistry Department, Faculty of Science, King Abdulaziz University, P.O. Box 80203, Jeddah 21589, Saudi Arabia

3 Department of Packaging, Yonsei University, Yonseidae-gil, Wonju 26493, Gangwon-do, South Korea

4 Center of Excellence for Advanced Materials Research, Faculty of Science, King Abdulaziz University, P.O. Box 80203, Jeddah 21589, Saudi Arabia

Heavy metals have adverse effects on the natural environment, aquatic life and human health. Due to non biodegradability, biological long half-lives and their potential accumulation in different body parts, heavy metals are toxic to human health. Some heavy metals are very toxic due to their solubility in water. Mercury among various heavy metals is one of the most toxic, carcinogenic pollutant in aqueous environment [13]. Mercury released into the aquatic environment by industries and other anthropogenic activities is most commonly the inorganic mercury. Inorganic mercury mostly occurs in monovalent Hg(I) and divalent Hg(II) cationic forms. As a kind of highly toxic, non-essential and non-biodegradable material, it may bio magnify through food chains. Even at very low concentration mercury have various adverse effects on aquatic plants and organisms. Several studies have shown that the brain, liver and gonad significantly accumulate mercury. Exposure to mercury mostly damage kidney, and may also causes morphological changes, proximal tubular necrosis, renal tubular damage and tubular epithelium regeneration [14, 15]. In aqueous solution, bacterial species can also convert water soluble divalent mercuric (Hg^{2+}) ions into organic mercury compounds methylmercury (MeHg) and ethylmercury (EtHg), which are found most commonly in fishes, and subsequently bio-accumulates in our body through the food chain [16]. Animal models reveal that MeHg is more carcinogenic and neurotoxic than EtHg. As compared to inorganic mercury, which mostly present free in plasma; MeHg is likely to bind with haemoglobin [17]. Besides these MeHg is a powerful neurotoxin and has been identified to cause serious health diseases including motor and sensory nerves damage [18]. Due to toxic and bioaccumulation effect, the monitoring of mercury ion level in the ecological samples is of high concern [19]. Numerous techniques have been used such as atomic fluorescence spectrometry, atomic absorption and atomic emission spectrometry and inductively coupled plasma spectrometry for the detection of mercury level in biological and environmental samples [20–23]. The available methods for detection of mercury have some limitations, including instrument maintenance, high analysis and instrumental cost, qualified operator and are time consuming. Sensitive, selective, cheap, quick and fields applicable methods are appreciable than available conventional methods [24, 25]. Due to numerous distinctive properties showed by AgNPs such as strong absorption and the scattering of light, high extinction coefficient (1×10^8 to 1×10^{10} $M^{-1}cm^{-1}$), localized SPR, detection of metal superiority than dyes, low cost, eco-friendly, colorimetric and simple naked eye detection, AgNPs prove to be a superior and an alternative to the conventional methods for detection of mercury [26]. For mercury sensing, plant mediated AgNPs have several advantages over chemically synthesized AgNPs such as the use of toxic chemicals as reducing agents, incorporation of

hazardous stabilizing agents, and need of high temperature and pressure. Plant mediated AgNPs are eco-friendly, low cost and synthesis at ambient temperature and pressure [24]. The diversity of secondary metabolites (glycosides, sterols, saponins, phenols, flavonoids, alkaloids, tannins, proteins and carbohydrates) obtained from fresh aqueous extract of *C. cneorum* made it the plant of choice.

In the present study AgNPs was synthesized using a fresh aqueous leaf extract of *C. cneorum* via novel green approach and their characterizations achieved using various analytical techniques. The main objective of the current study is to use the freshly prepared *C. cneorum* leaf mediated AgNPs for selective and specific detection of Hg^{II}, Cr^{VI} and aqueous ammonia.

2 Experimental

2.1 Materials

Silver nitrate, mercuric sulphate and potassium dichromate were purchased from Merck (Germany). Lead nitrate, chromic nitrate, cadmium sulphate, nickel nitrate, cobaltous sulphate, zinc acetate, ferrous sulphate and copper sulphate were from BDH chemicals England. The solvent aqueous ammonia and ethanol used were of analytical grade. All experiments were performed in triplicate.

2.2 Preparation of leaf extract

For preparation of aqueous extract fresh leaves of *C. cneorum* were used. About 20 g of *C. cneorum* leaves were taken and washed with tap water followed by washing with double distilled water, air dried, and then crushed into 100 mL deionized water using electric blender. For preparation of leaf extract the mixture was heated in a water bath at boiling temperature for 30 min. The extract was then filtered through Whatman No. 42 filter paper and used for further process.

2.3 Synthesis of silver nanoparticles

For synthesis of AgNPs 80 mL of 10 mM aqueous silver nitrate ($AgNO_3$) solution was taken in conical flask and introduced 20 mL of freshly prepared aqueous extract of *C. cneorum* at room temperature. The color change was observed from yellowish to dark red instantly after the addition of leaf extract to $AgNO_3$ solution. The prepared nanoparticles were then centrifuged at 4000 rpm for 10 min. The resulting pellets of AgNPs were washed with double distilled water; centrifuged again followed by washing with absolute ethanol. The resulting product was dried at room temperature [27].

The kinetics of the reaction was studied by varying the concentration of silver nitrate, plant extract and also at different temperature. To study the effect of silver nitrate, different concentration of 5, 10, 15, 20, 25 and 30 mM AgNO₃ solutions were treated with a 20 mL of plant extract at room temperature and monitored by UV–visible spectrophotometer. For the study of the effect of plant extracts, various concentration of 5, 10, 15, 20 and 30 mL were treated with 10 mM silver nitrate. While the temperature effect was evaluated at a constant concentration of silver nitrate and plant extract, i.e., at 30 °C, 40 °C, 50 °C, 60 °C and 70 °C. The synthesis of AgNPs was monitored with different time 20, 40, 60, 90 and 120 min, and also studied their stability after 24 and 48 h and 2 weeks.

2.4 Optical sensing of ammonia, mercury and chromium ions

Optical detection of hexavalent chromium, divalent mercuric ions, aqueous ammonia and other heavy metal ions were evaluated through freshly prepared AgNPs using the UV–visible spectrophotometer Shimadzu, UV-1800 (Japan). To investigate the prepared AgNPs interaction with different metals like Pb^{II}, Cr^{VI}, Cr^{III}, Cd^{II}, Ni^{II}, Co^{II}, Hg^{II}, Zn^{II}, Cu^{II} and Fe^{II}, about 200 ppm stock solution of these metal ions were prepared. The same concentration of ammonia solution was also prepared. After selectivity of Cr^{VI}, Hg^{II} and aqueous ammonia, a detailed study of these three species was carried out.

For sensing of Hg^{II} 4 mL quartz cuvette was used as reaction vessel. For reaction about 1.5 mL of freshly prepared AgNPs was introduced into a cuvette and then added 1.5 mL of different concentration of (5, 10, 50, 100 ppb and 1, 5, 10, 20, 50, 100 and 150 ppm) of Hg(II) solution. The decrease in intensity and changes in absorbance peaks at 452 nm of AgNPs after 3 min of the addition of Hg^{II} was monitored by UV–visible spectrophotometer with different time intervals. The same procedure was used for sensing aqueous ammonia. Different concentrations of ammonia were used for sensing procedures, as follows: 5, 10, 50, 100, 200, and 300 ppm.

2.5 Cellulose filter paper based detection of ammonia and mercury ions

Naked eye detection of aqueous ammonia and Hg^{II} were carried out by using filter paper doped AgNPs. The cellulose filter paper based AgNPs strips (CF-AgNPs) were prepared by dropping the colloidal solution of freshly prepared silver nanoparticles on 20 different strips of Whatman filter paper no. 1 (spot drop area 15 mm²), followed by air drying at normal temperature for 10 min. These CF-AgNPs strips were then used for the detection of Hg^{II} and aqueous ammonia. For this, different concentrations of mercuric sulphate

(50 μM to 50 mM) and aqueous ammonia (10 μM to 50 mM) were prepared. For the detection, the strip was suspended in 3 mL solution of Hg^{II} and ammonia using quartz cuvette and noted the decolorization time. In control experiments, same volume of de-ionized (DI) water was used. Each test was performed in triplicate.

2.6 Characterizations of silver nanoparticles

For measurements of surface plasmon resonance of *C. cneorum* mediated AgNPs, UV–visible spectrophotometer Shimadzu, UV-1800 (Japan) was used. In order to characterize the functional groups on the AgNPs surface FT-IR spectral measurements were carried out at on a spectrum-100 FT-IR spectrophotometer purchased from Bruker (ALPHA, USA) using a KBr pellet method for nanoparticles within a fixed spectral range, i.e. 4000–400 cm⁻¹. For surface morphology, size and shape of the prepared AgNPs, JEOL (JSM-7600F, Japan) FE-SEM instrument was used. For confirmation of elemental analysis (EDX) JEOL (JSM-7600F, Japan) system was used. XRD measurement was used to check crystallinity and to measure the average crystallite size of prepared nanoparticles. The nanoparticles were investigated using a JDX-3532 JEOL JAPANX-ray Diffractometer (40 kV, 30 mA, monochromatic) using a Cu K alpha source (1.5418 Å). The scanning range used for the sample analysis was $20° \leq 2\theta \geq 70°$ with a scanning rate of 0.5 s per step and a step size of 0.05°. The average size of the prepared nanoparticles was calculated by using Scherrer equation.

$$L = k\lambda/\beta_{1/2}\cos\theta \tag{1}$$

Where θ shows the Bragg's angle and λ indicate the wavelength (1.5418 Å) of the used X-rays, $\beta_{1/2}$ is the full peak width at half maximum (FWHM) in radians on 2θ scale, and k is the constant which is related to the crystal shape and the way in which θ is defined and approximately equal to unity.

3 Results and discussion

3.1 UV–visible analysis of silver nanoparticles

In the present work, aqueous leaf extract of *C. cneorum* was used for synthesis of stable AgNPs. Nanoparticles formation was confirmed by a change in color of the solution mixture from light yellow to dark red (Fig. 1) and the spectra of AgNPs was monitored using UV–visible spectrophotometer. UV–visible absorption spectrum was recorded after 30 min of the reaction, which show maximum absorbance at 452 nm as shown in Fig. 2d. The absorption at 452 nm shows the formation of AgNPs [28]. It has been reported in the literature that silver show SPR from 440 to 460 depending upon their size [29, 30]. The excitations of electrons on the surface of

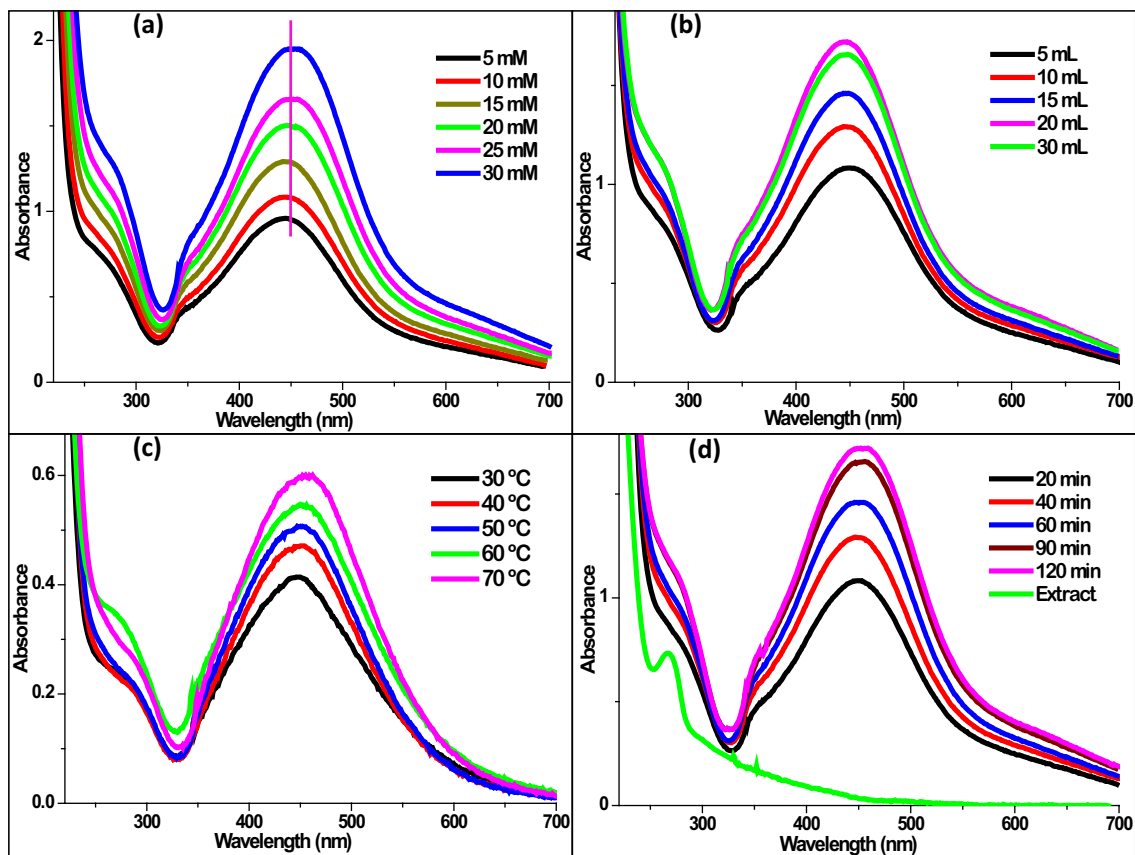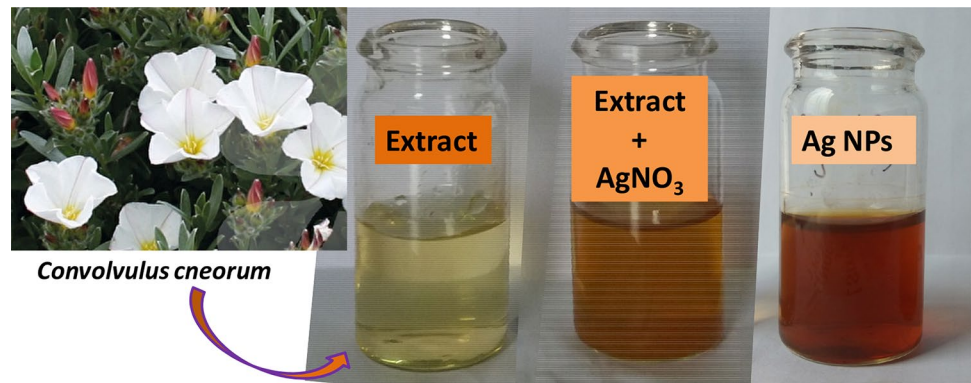**Fig. 1** Schematic representation of Ag NPs synthesis

Fig. 2 UV–visible spectra of **a** change in the SPR band of Ag NPs at different concentration of AgNO$_3$ (5, 10, 15, 20, 25 and 30 mM), **b** change in the SPR band of Ag NPs at various amounts of plant extract (5, 10, 15, 20 and 30 mL), **c** change in the SPR band of Ag NPs at different temperature (30 °C, 40 °C, 50 °C, 60 °C and 70 °C) and **d** change in the SPR band of Ag NPs with time

nanoparticles in their conduction band in resonance with light wave are collectively called surface plasmon resonance of nanoparticles. The SPR band of AgNPs remains close to 450 nm all over the reaction period. The stability of the SPR band in the solution confirmed that the particles are monodispersed in their aqueous phase with no sign of agglomeration. The stability of nanoparticles could be due to the capping or stabilizing agent which probably may be proteins, especially amino acids of proteins present in the

plant extract into the reaction medium [31]. Here we report fresh aqueous leaves of *C. cneorum* extract AgNPs, which is single step, less laborious and faster as compared to the previously reported *C. arvensis* mediated AgNPs, in which 1 week shade dried leaves were used [32]. The previously reported shade dried synthesizing method is complicated and time-consuming (~ 3 h).The reduction time of silver using fresh aqueous extract was faster (less than 1 h) than the dried leaf extract of *C. arvensis*. The prepared AgNPs

showed excellent stability with no sign of aggregation and a shift in the SPR. The effect of variation in the plant extract (reducing material), silver nitrate concentration and temperature of synthesis of nanoparticles has been studied.

3.1.1 Effect of silver nitrate

The effect of silver nitrate concentration on the formation of AgNPs has been studied. UV–visible spectra of the prepared AgNPs at different silver nitrate concentration (5, 10, 15, 20, 25 and 30 mM) have been shown in Fig. 2a. As shown in Fig. 2a with increase in silver nitrate concentrations from 5 to 30 mM, the rate of AgNPs formation also increases with the shift of the SPR band from 442 to 453 nm and simultaneous band broadening of the reaction medium. The spectrum of AgNPs exhibit red shift, which indicate the formation of larger size particle and the broadening of band show irregular shape particles with aggregation [33]. It has been reported in the literature that the SPR band shifted towards lower wavelength (blue shift) when electrons are donated to the nanoparticles and shifted towards higher wavelength (red shift) when holes are inserted to the clusters [34, 35].

The SPR absorbance peak of AgNPs was found to be higher at elevated concentrations of silver solution. Increasing the amount of metal ions concentration from 5 to 30 mM increases the rate of reduction by formation of a large number of nuclei with the enhanced SPR absorption band as shown in Fig. 2a. The synthesis of AgNPs was found low at lower silver nitrate concentration.

3.1.2 Effect of plant extract

The effect of plant extract on the formation of AgNPs was also studied. Figure 2b indicates the UV–visible spectra of synthesized AgNPs at various concentrations of *C. cneorum* leaf extracts. Figure 2b signifies the role of plant extract in the formation of AgNPs. As previously reported that, the role of reducing as well as capping agents are very important in the synthesis of nanoparticles. In the present study, upon increasing the amount of leaf extract; consequently the change in color was observed from yellowish to dark red, which show the formation of AgNPs. The SPR peak of AgNPs depends on the concentration of plant extract, and become sharper at elevated concentration. It was observed that with increasing the amount of leaf extract from 5 to 20 mL the SPR absorption band for AgNPs increases as shown in Fig. 2b. However, at an amount of 30 mL leaf extract the absorption band at 452 nm decreases, which may be due to the fact that high concentration of a leaf extract causes turbidity and the resulting nanoparticles are not fully exposed to the light. The position of a localized SPR band of metallic nanoparticles depends on their size and shape [34]. As observed that increasing the concentration of leaf extract,

λ_{max} value increases with blue shift from 458 to 450 nm. This observed blue shift indicates the decrease in the mean diameter of the AgNPs. The blue shift in higher concentration from 5 to 20 mL and sharpening of SPR peak show the formation of small size spherical AgNPs. By increasing the amount of leaf extract thereby increasing the rate of reduction due to the presence of a large number of biomolecules for reduction, which increase the intensity, and decrease the size due to the availability of a large number of capping agents which cover the nanoparticles surface. Based on the above results, it was concluded that the concentration of the plant extract plays central role in the formation of AgNPs.

The variety of secondary metabolites (phenols, sterols, flavonoids, saponins, tannins and alkaloids etc) present in the fresh aqueous extract of *C. cneorum* is responsible for the reduction of Ag nanoparticles. A plausible mechanism is given in Scheme 1.

3.1.3 Effect of temperature

The effect of temperature on the biosynthesis of AgNPs was studied after 30 min of the reaction at various temperature as shown in Fig. 2c. The intensity of SPR peak increases by increasing the reaction temperature from 30 to 70 °C, which shows that the rate of formation of AgNPs increases with red shift from 451 to 457 nm and simultaneous broadening of a localized SPR band of synthesized nanoparticles. Most likely at elevated temperature the rate of reaction increases that occurs due to increasing molecular motion and the conversion of the Ag$^+$ ions to Ag nanoparticles [36]. The shift in peak positions from 451 to 457 nm shows the formation of larger size particles.

3.1.4 Effect of time on synthesis

In the present study, 20 mL leaf extract of *C. cneorum* in the presence of 10 mM silver nitrate solution shows better production of smaller size AgNPs at ambient temperature. Temperature and incubation time significantly control the process of AgNPs synthesis. Synthesis of AgNPs was evaluated at different interval of reaction time using UV–visible spectrophotometer. Figure 2d show UV–visible spectra
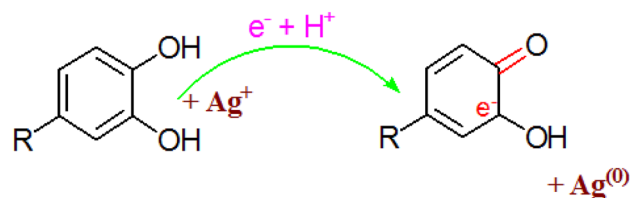
Scheme 1 Plausible mechanism of the reduction of silver ions by phytoconstituents of the plants extract

of synthesized AgNPs at different time interval (20, 40, 60, 90 and 120 min).

The characteristic localized SPR band at 451 nm for silver colloids increases with times which show the formation of nanoparticles. As shown in Fig. 2d the peak position at 451 nm started within time of 20 min and increased up to 2 h. This study demonstrates that the AgNPs prepared by green synthesis method shows excellent stability without aggregation. Thus, our prepared fresh aqueous extract *C. cneorum* mediated AgNPs takes less time (90 min) and showed a faster reduction than previously reported *Convolvulus pluricaulis* mediated AgNPs which took 10 h of incubation for the complete reduction of silver ions to AgNPs [37]. Aqueous leaf extract of *C. cneorum* gives absorption peak at 261 nm in the UV region (Fig. 2d) which might be due to the presence of aromatic amino acids of protein, especially tyrosine and tryptophan and, to a some extent, the disulfide bonds between cysteine residues [38].

3.1.5 Stability of AgNPs

The stability of prepared AgNPs was measured by evaluating the optical spectra of the prepared nanoparticles recorded after 20 min to 4 months, since the stability of nanoparticles is one of the essential parameters. The formation of AgNPs started within 5 min from the observed change in color from light yellowish to dark red and the intensity of the SPR peak increased up to 48 h, after which no color change was observed, but slight variation and broadening of SPR peak position at 451 nm up to 14 days. The AgNPs prepared by this method were continuously monitored at room temperature upto 4 months and were found stable and no peak distortion or deformation was observed. The variation and broadening of SPR peak from 442 to 461 nm as shown in Fig. 3, might be due to the slight aggregation of AgNPs and the formation of larger size particles. Thus it could be concluded that *C. Cneorum* mediated AgNPs are quite stable in aqueous solution for longer time even up to 4 months.

Thus, from the above observations, it was concluded that 20 mL plant extract with 10 mM AgNO$_3$ solution after 90 min gave the highest yield at optimum conditions for the green synthesis of AgNPs even at room temperature. The yield could be increased at higher temperature, however in order to stick to the atom economy of green chemistry, the results of the product at room temperature are outstanding. Besides at elevated temperature the observed red shift in the surface plasmon resonance suggest the increase in particles size. That is why at room temperature smaller size particles formation occur.
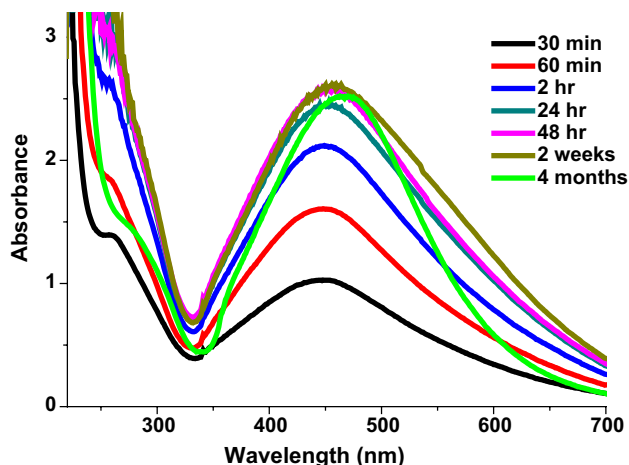

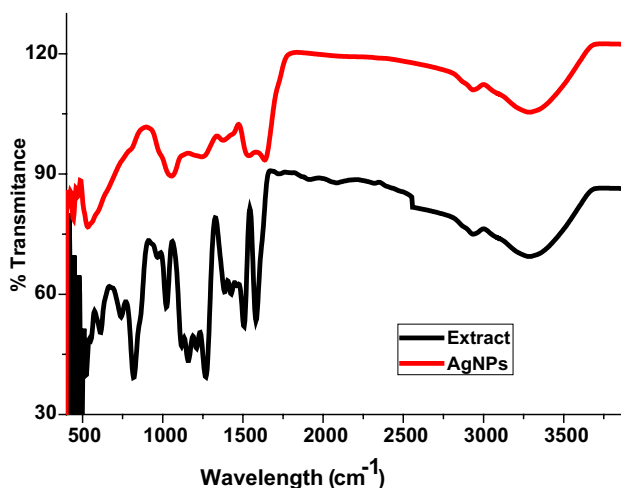**Fig. 3** UV–visible spectra showing the stability of synthesized Ag NPs

Fig. 4 FT-IR spectrum of a *C. cneorum* fruit extract and Ag NPs

3.2 FT-IR spectrum of silver nanoparticles

For identification of capping, stabilizing as well as reducing agents, FT-IR analyses of the prepared AgNPs were performed. The main absorbance bands in the spectrum of *C. cneorum* extract were at 3386, 2955, 1560, 1412, 1276, 1168, 1029 and 830 cm^{-1}. However, synthesized AgNPs show bands at 3332, 2966, 1647, 1558, 1260, 1071 and 563 cm^{-1} as shown in Fig. 4. The broadband observed from 3320 cm^{-1} is the characteristic of alcohols and phenolic compound hydroxyl functional group and various carbonyl functional groups of the extract [39, 40]. The small band at 2966 cm^{-1} may be rise due to the stretching vibrations of methylene groups [41, 42]. The bands at 1647 and 1558 cm^{-1} is the characteristic bending vibrations of amide I and amide II linkages of the extract

proteins, respectively [43, 44]. The observed bands at 1412 cm^{-1} could be assigned to the C–N stretching vibrations mood of aromatic amines [45]. The sharp peak at 1260 cm^{-1} corresponds to the C–O stretching vibration of carboxylic acids [42]. The peak at 1065 cm^{-1} corresponds to the C–N aliphatic amines stretching vibrations [43]. A strong peak at 830 cm^{-1} could be assigned p-disubstituted benzene [46, 47]. A strong peak observed at 563 cm^{-1} may be corresponds to the ligand–metal stretching frequency which be arise due to the capping of biomolecules on the nanoparticles surface [45].

In case of spectrum of AgNPs (Fig. 4), all peaks of plant extract usually amino acids were present along with new peak at 555 cm^{-1} which are corresponding to the M–O bond representing the interaction of Ag nanoparticles with surface capping agents and confirm the formation of nanoparticles [48]. The overall observations obtained from FT-IR study has confirmed that the proteins residues, especially amino acids have stronger capability to bind with metal and act as capping ligands of AgNPs and prevent them from aggregation. Thus, it is concluded from the above observation that the biological molecules (protein, alcohols and phenolic compounds) could probably perform the function of both reductions as well as capping/stabilization agents of the AgNPs in aqueous medium.

3.3 FE-SEM and EDX analyses of silver nanoparticles

FE-SEM images of *C. cneorum* synthesized AgNPs is shown in Fig. 5 and were found to be a spherical shape with no sign of aggregation. It has been confirmed from FE-SEM images also that the prepared nanoparticles are capped by biomolecules as the edges of the nanoparticles are looking rough. The FE-SEM images of the nanoparticles show that the shape of AgNPs is mostly spherical and oval and are monodispersed. The size of the *C. cneorum* extract synthesized AgNPs determined from FE-SEM images were found in the range of 18–26 nm (mean diameter of about $\sim 22 \pm 4$ nm) and are monodispersed lacking aggregation. The formation of nanoclusturs may be due the presence of elevated concentrations of biological active molecules in the colloidal solution. It has been reported that optical and electronic properties of the metal nanoparticles have considerably changed by changing the shape of the nanoparticles [49].

For confirmation of elemental analysis, the prepared nanoparticles were subjected for EDX, giving an additional
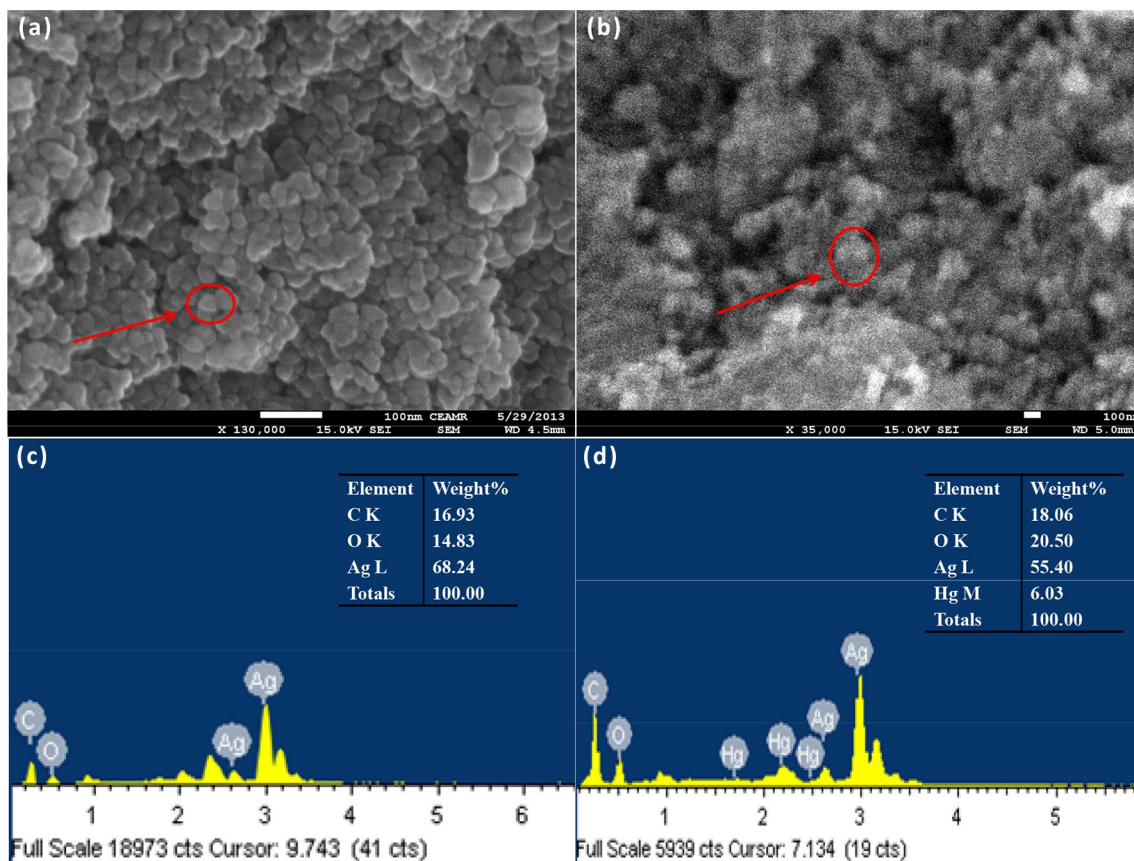

Fig. 5 **a** FE-SEM image of Ag NPs **b** FE-SEM image after Hg^{II} sensing, **c** EDX analysis of Ag NPs and **d** EDX analysis after Hg^{II} sensing

confirmation for the reduction of silver ions to elemental nanosilver. The graph of EDX analysis as shown in Fig. 5c proves the presence of elemental silver, which support the UV–visible results, and confirm the reduction of silver ions into AgNPs. The crystalline natures of AgNPs are clearly shown from the EDX pattern, which is reduced by *C. cneorum* extract from silver ions. A strong signal peak for silver was observed at 3 keV, which confirm the formation of AgNPs. Due to localized SPR, metallic silver usually shows absorption peak approximately at 3 keV [50, 51]. The weight percentages of the specific elements in AgNPs were 68.24% Ag, 14.83% O and 16.93% C as shown in Fig. 5c. The spectrum also shows weak signals for carbon and oxygen, which may be arising from the organic molecules capping the surface of AgNPs.

The weight percentages after sensing with mercury of the specific elements were 55.4% Ag, 6.03% Hg, 20.5% O and 18.06% C as shown in Fig. 5d. EDX investigation after Hg^{II} sensing showed the specific signal peak for mercury, which confirmed the formation of silver-amalgam.

3.4 XRD spectrum of silver nanoparticles

The XRD patterns of biosynthesized AgNPs (Fig. 6) showed three strong peaks in the spectrum of 2θ value from 20 to 70. In XRD patterns the three distinct diffraction peaks at the 2θ position of 38.1, 44.29 and 64.43 corresponding to characteristic Bragg peaks of (111), (200) and (220), which correspond to the face centered cubic crystal structure of AgNPs [52, 53]. The average particle size of the nanoparticles was calculated from the XRD data using Scherrer equation from the FWHM of the most intense peak. The average particle size of AgNPs was thus found about $\sim 27 \pm 6$ nm, ably supported by FE-SEM analysis too. These results indicate that AgNPs synthesized using *C. cneorum* leaf produced crystallite in nanosize.
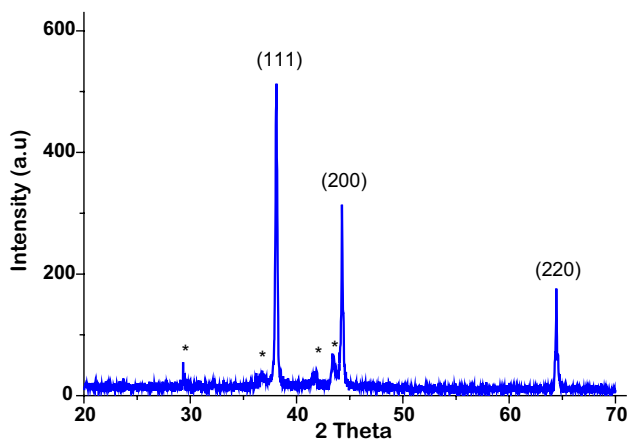

Fig. 6 XRD pattern of *C. cneorum* mediated Ag NPs

3.5 Sensing study and selectivity

The color changes of nanoparticles solution were monitored using UV–visible spectrophotometer after the individual addition of 200 ppm solution of ammonia and other toxic heavy metal ions. The UV–visible spectra of individual species were recorded after 5 min. The change in color of AgNPs solutions is shown in Fig. 7c, d. The prepared Ag NPs were interacted with the aqueous solutions containing different heavy metal ions Hg^{II}, Cr^{VI}, Zn^{II}, Cd^{II}, Pb^{II}, Fe^{II}, Co^{II}, Cr^{III}, Cu^{II} and Ni^{II}. The photographs as shown in Fig. 7c, d and UV–visible spectra Fig. 7a of AgNPs were taken after addition of metal ions, after 5 min of interaction with nanoparticles. AgNPs did not show colorimetric sensing property towards any cations except Hg^{II} and Cr^{VI} and ammonia. The dark brown color of the AgNPs showed a distinctive change in color only in response to the ammonia, Hg^{II} and $(Cr_2O_7)^{2-}$ ions. The selective detection of Hg^{II} and $(Cr_2O_7)^{2-}$ ions is due to the electrochemical differences of heavy metal ions and Ag^0. Those metals which have high reduction potentials act as an oxidizing agent and could be detected via colorimetric sensing using UV–visible spectrophotometer. Since Hg^{II} and $(Cr_2O_7)^{2-}$ ions have higher reduction potential of $+0.85$ V and $+1.33$ V respectively, than Ag(0) which has reduction potential of $+0.8$ V, and thus they can oxidize Ag(0) to Ag^I ions and get reduced [54].

It was also observed that the addition of Cr^{III} (-0.74), Zn^{II} (-0.76), Pb^{II} (-0.13), Cd^{II} (-0.40), Co^{II} (-0.28), Cu^{II} ($+0.34$), Fe^{II} (-0.44), and Ni^{II} (-0.26) cations to AgNPs solution did not show any significant changes in their color or SPR. Thus, none of the above metals have high reduction potentials than silver and can't act as an oxidizing agent. Therefore, colorimetric detection of them is not possible via AgNPs.

However, the addition of ammonia to the colloidal solution of AgNPs, the complex $(Ag(NH_3)_2^+)$ formation occurs between Ag^+ and NH_3, which in turn the surface charge of silver colloids increases and create repulsion force between nanoparticles.

3.5.1 Colorimetric sensing of Hg(II)

Mercury is the most toxic and carcinogenic elements and is categorized as a global pollutant. Exposure of mercury by both anthropogenic and natural activities are considered as the highest risk to our aqueous environment [55]. The increasing concentration of mercury in natural environment is due to the combustion of fossil fuel, coal, oil and their by-products [56]. Mercury can be absorbed through the food chain or inhaled by the mucous membranes in the human body [57]. Compounds of inorganic mercury mainly produce toxic effects on kidney in both laboratory animals and humans following short and long term exposure. In
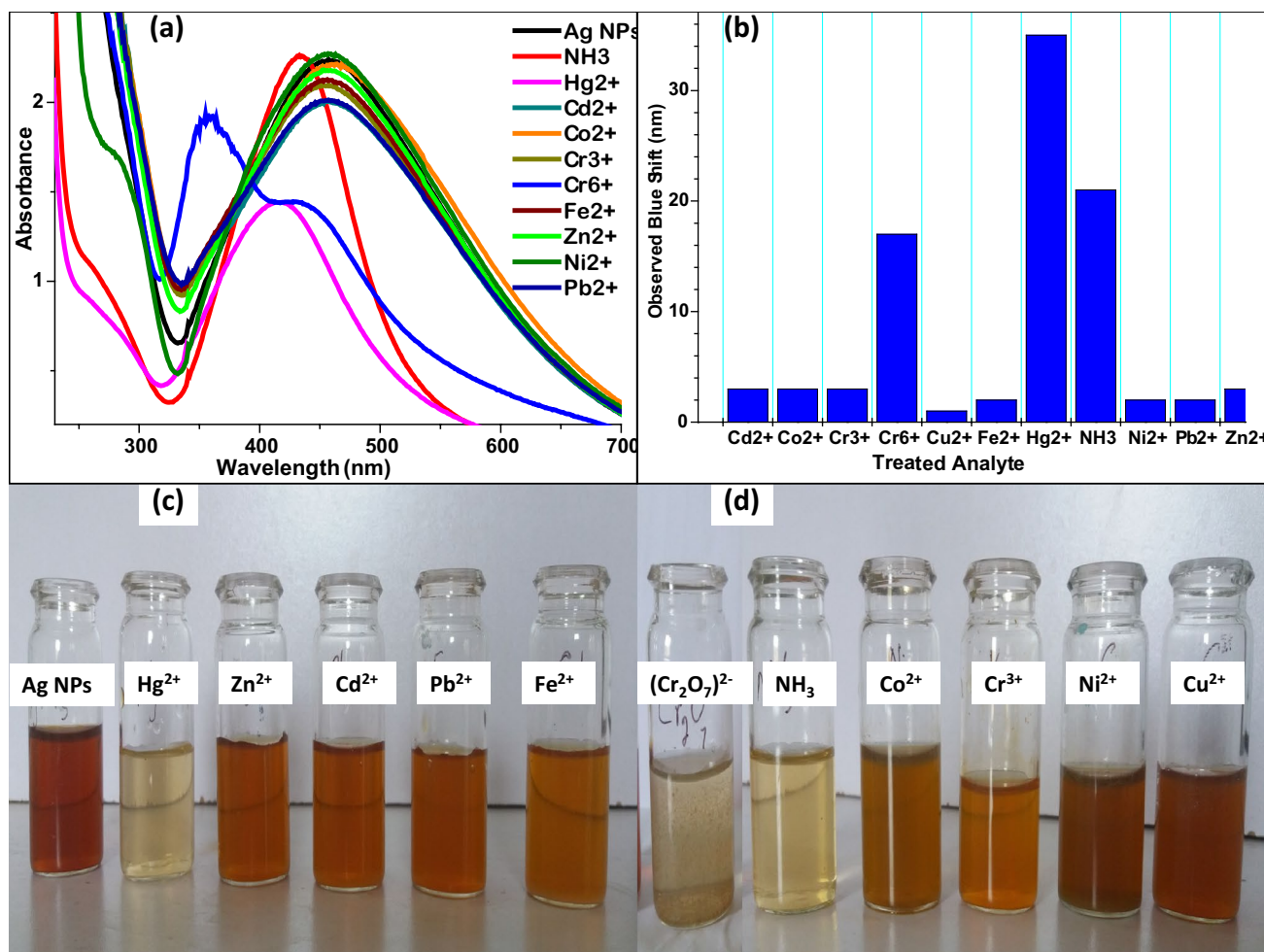
Fig. 7 UV–Vis spectra **a** Ag NPs in the presence of NH_3, Hg^{2+}, Zn^{2+}, Cd^{2+}, Pb^{2+}, Fe^{2+}, Co^{2+}, Cr^{3+}, Cr^{6+}, and Ni^{2+} **b** histogram showing blue shift after 20 min treatment with Ag NPs **c, d** visual representation of color change by different treated analyte

rats, exposure to mercury causes increased in relative and absolute kidney weights, tubular proteinuria, necrosis and hypoalbuminemia. While oral exposure to humans' causes acute poisoning, which results primarily in colitis and haemorrhagic gastritis; the ultimate damage is the kidney [58]. Beside, some toxic hydrophobic organic compounds of Hg^{II} can easily cross the biological membranes, thereby increasing Hg^{II} level in the blood and have direct and long lasting effect on central nervous system [59].

Mercury enters into our body through the food chain in the form of organic mercury. Fish consumption appears to be the main source of organic mercury. Due to its solubility in fats, methyl-mercury can easily cross the placenta and potentially affect the fetus health [60]. In the environment, mercury pollution comes from the burning of coal and municipal solid wastes. The total mercury in the water phase has been reported to differ widely from 10 to 300 ppb. In the water phase, the major species of mercury exists in inorganic form ($HgCl_2$) [61]. The major ways of mercury

pollution in the environment are untreated water which is released from different industrial process and natural gas and petroleum refining.

Therefore, the development of simple methods for detection of Hg^{II} is necessary. The prepared AgNPs was tested for colorimetric determination of mercury ions. Due to the strong SPR absorption band in the visible region of AgNPs; it would be simple and easily examine the changes in the local SPR band of AgNPs in the determination of Hg^{II}. For measurement of Hg^{II}, different dilutions of mercuric sulphate i.e., (5, 10, 50 and 100 ppb) and (1, 5, 10, 20, 50, 100 and 150 ppm) solution were prepared. For sensing 1.5 mL of Hg^{II} solution was introduced in a quartz cuvette containing 1.5 mL freshly prepared AgNPs solution and the change in optical property of AgNPs monitored using UV–visible spectrophotometer. Figure 8a, b shows the change in the SPR absorption band for AgNPs upon addition of 1.5 mL of various concentrations of Hg^{II} solution. A considerable decrease in the intensity of the SPR band of AgNPs was observed
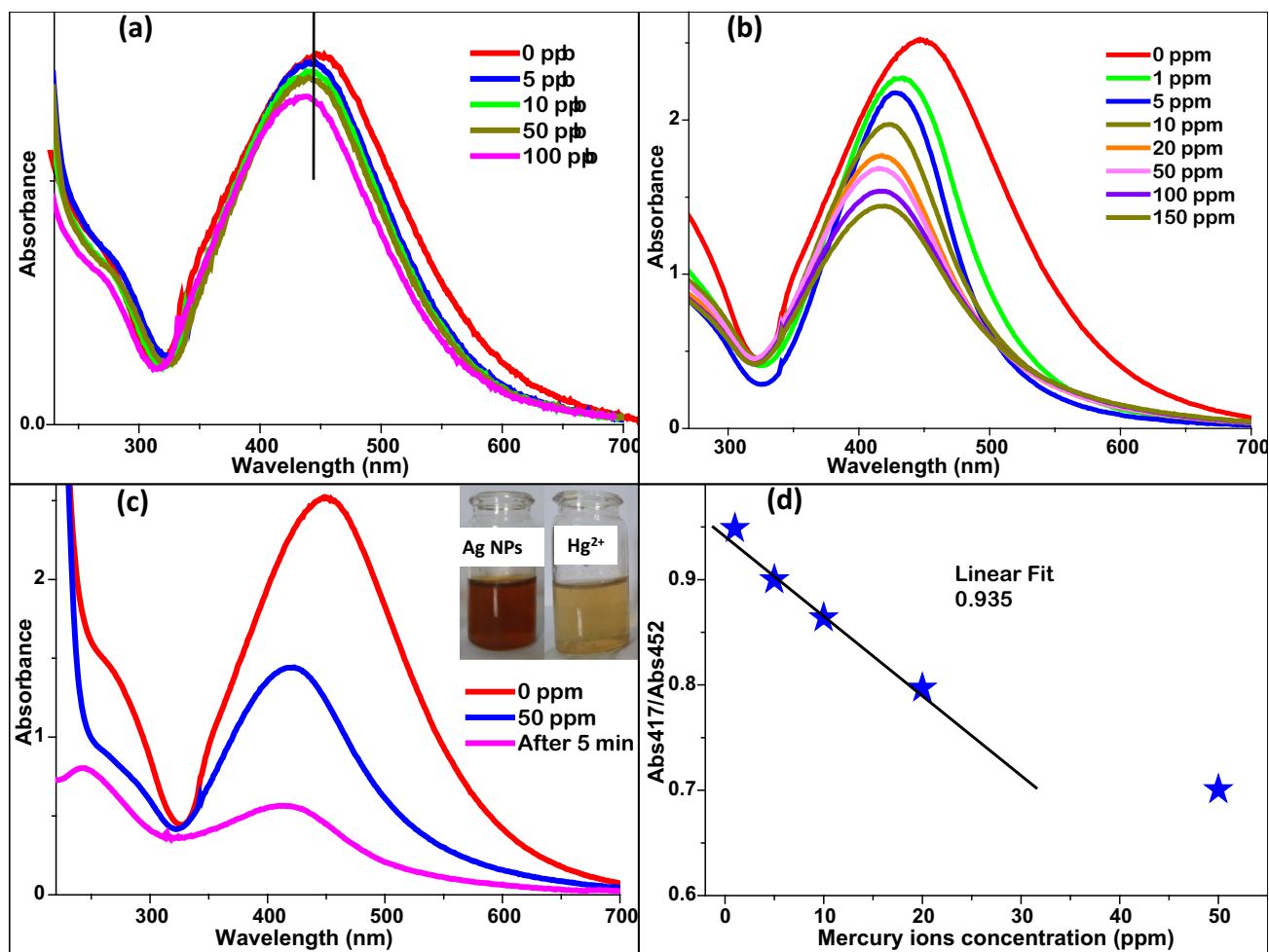
Fig. 8 **a** The plot of changes in UV–visible spectra in colloidal solution of Ag NPs as a function of different concentration of Hg^{II} (5, 10, 50 and 100 ppb), **b** the plot of changes in UV–visible spectra of Ag NPs as a function of Hg^{II} concentration of (1, 5, 10, 20, 50, 100 and 150 ppm), **c** effect of time on UV–visible spectra of Ag NPs after addition of Hg^{II} (inset show the change in color after the addition of Hg^{II} solution), and **d** ratio of the absorbance peaks at 417 and 452 nm giving algorithmic curve as a function of Hg^{II} concentration (1–20 ppm) with a correlation factor R^2 = 0.935

with a blue shift in λ$_{max}$. The absorption band of prepared AgNPs decreases by increasing Hg^{II} concentration.

The observed shift in the SPR of AgNPs from 452 nm was 447, 445, 442 and 438 nm for 5, 10, 50 and 100 ppb respectively. However above 500 ppb significant decline in the absorption intensity and shift from 452 to 417 nm was observed for Hg^{II} concentration. This phenomenon of Hg sensing was consistant with the previous studies [62, 63].

The mechanism of Hg^{II} sensing by AgNPs could be explained on the bases of electrochemical differences of Hg^{II} and Ag^{I}. The significant shift and finally disappearance in the absorption intensity of AgNPs was due to the differences in redox interaction and the electrochemical property between AgNPs and Hg^{II} ions. The decrease in the SPR absorption intensity may be due to the oxidation of AgNPs. Since the standard reduction potential of Hg^{II}

is higher + 0.85 V than Ag(0) which has reduction potential + 0.8 V, and thus Hg^{II} oxidize Ag(0) to Ag^{I} ions and get reduced to Hg(0) [54]. EDX investigation of this product was depicted in Fig. 5d. EDX analysis of AgNPs after sensing showed that the concentration of silver decreases. This may be due to the oxidation of Ag(0) to Ag^{I} and the formation of silver oxide. While the gradual blue shift in the SPR band of AgNPs from 452 to 417 nm could be attributed due to adsorption of Hg^{II} on the surface of AgNPs, resulting in the disintegration of the AgNPs into smaller particles and thereby the formation of Ag-amalgam particles [64, 65]. There is very strong affinity between silver and elementary mercury [63, 66], elementary Hg could be easily adsorbed on the nanoparticles surface by forming Ag-Hg, leads in the decrease in charges on AgNPs surfaces, which results to the enlargement/aggregation of AgNPs which was observed

from our FE-SEM results. The FE-SEM image of pure and Hg treated AgNPs clearly shows that the sizes of particle increases after the addition of Hg^{II} to AgNPs [62].

Thus, it can be concluded that Hg^{II} firstly adsorbed on nanoparticles surface due to which shift is observed and then gradually start oxidation of AgNPs due to which decrease in λ_{max} occur with time (Fig. 8c). The plot of the ratio of absorption intensity of tow difference value (abs417/abs452) against various concentrations of Hg^{II} showed a logarithmic curve with a correlation factor $R^2 = 0.935$ in the concentration range of 1–50 ppm (Fig. 8d). The absorbance ratio gives linear relationship with the Hg^{II} concentration in the range of 1–50 ppm. Beyond 20 ppm of Hg^{II} concentration, the ratio become constant to some extent, which demonstrate that the optical sensor based on AgNPs is more active and got more attention for detection at lower concentration of Hg^{II} content in water sample as compared to the recently reported literature 10-alkylacridinium-based chemosensors which detected up to 10 ppm [67], graphene oxide-silver nanocomposites 0.59 ppm [68], and silver nanoparticles 2 ppm [69].The WHO guideline for drinking-water of mercury is 6 μg/L [70]. However, United State Environmental Protection Agency (US-EPA) national primary drinking water regulations guideline value for mercury is 5 μg/L [71, 71].

Thus, the detection limit of prepared AgNPs (5 ppb) for Hg^{II} demonstrated the lowest possible limits for WHO and US-EPA guideline for drinking-water.

3.5.2 Sensing of ammonia

Animal wastes and agricultural fertilizers are the primarily sources of anthropogenic ammonia. For atmospheric ammonia agriculture is the main source which account for 55–56% of global ammonia emission [72]. Ammonia also enters into the aqueous environment through different manufacturing processes, mainly through the use of pesticides, explosives, textiles, dyes, plastics and cleaning solutions [73]. The lifespan of ammonia is less than 5 days and extended up to 10 days when converted into aerosols of ammonium, which leads to eutrophication and acidification of water. Thus, to reduce the concentration of ammonia in water bodies below the recommended standards of the WHO, US-EPA and a European environment agency motivated the scientist to develop methods for removal of ammonia.

The sensing for ammonia solution was carried out by the optical measurement using UV–visible spectrophotometer. The changes in SPR spectra of prepared AgNPs were studies with various concentrations of ammonia, i.e., (5, 10, 50, 100, 200, and 300 ppm) as shown in Fig. 9a. The changes in absorbance value of AgNPs were recorded as a function of ammonia concentration. For sensing freshly prepared AgNPs was used. As shown in Fig. 9a that SPR intensity of AgNPs increases with blue shift with increasing

the ammonia concentration from 5 to 300 ppm. The shift in peak occurs from 452 to 431 nm. Thus, the absorption spectra at 431 nm can be analyzed easily and the ammonia concentration can be detected. The shift in the absorption peak of AgNPs may be due to the association of Ag^+ ions with ammonia form a coordination complex $Ag(NH_3)_2^+$. It has been reported in the literature that addition of ammonia to the colloidal solution of AgNPs, the complex $(Ag(NH_3)_2^+)$ formation occurs between Ag^+ and NH_3, which in turn the surface charge of silver colloids increases and create repulsion force between nanoparticles. Beside these upon the addition of ammonia to AgNPs solution, the variation in dielectric constant of the surrounding medium occurs and in the inter-particles distance changed [74]. This results in the formation of more hydrophilic and isolated particles with a blue shift spectrum. The changes in SPR at two different wavelengths of AgNPs with gradual decrease as a function of ammonia concentration are provided in Fig. 9b. The kinetics of the reaction were taken by processing the data and taking the ration of the absorbance ratio of (Abs431/Abs452) vs ammonia concentration as shown in Fig. 9c. The relative change in absorbance gives an excellent linear correlation from a concentration of 5 to 300 ppm with a correlation factor R^2 equal to 0.968 which is comparable to the previously reported literature [74, 75]. The taste threshold concentration at alkaline pH for ammonia is about 35 ppm and 25 ppm for short term exposure while the odour threshold concentration is about 1.5 mg/L, has been proposed for the ammonium. The presence of ammonia in water at these levels is not of direct relevance to the health, and thus, no health-based guideline value for the drinking water has been proposed [70, 76].

3.5.3 Cellulose filter paper based sensor of Hg^{II} and ammonia

For deployability in the field, the prepared nanoparticles were employed on cellulose filter paper to form filter paper based silver nanoparticles (CF-AgNPs) probe for the detection of Hg^{II} and ammonia in aqueous solution. Such CF-AgNPs probe will able us in the field for naked eye detection of Hg^{II} and aqueous ammonia.

Figure 10 illustrates the photographic images taken after the decolorization or disappearance of the red color spots of AgNPs on cellulose acetate filter paper after treating with Hg^{II} solution. At 50 mM Hg^{II} concentration, the AgNPs spot disappeared just after the addition of Hg^{II}. For 10 and 5 mM Hg^{II} concentration, the AgNPs spot disappeared after 1 and 8 min respectively. Similarly for 1 and 0.5 mM Hg^{II} concentration, the decolourization of AgNPs took 15 and 20 min respectively. Decolourization of 200 and 100 μM Hg^{II} solution took 25 and 30 min respectively. At lower concentrations of 50 μM Hg^{II} concentration, decolourization of
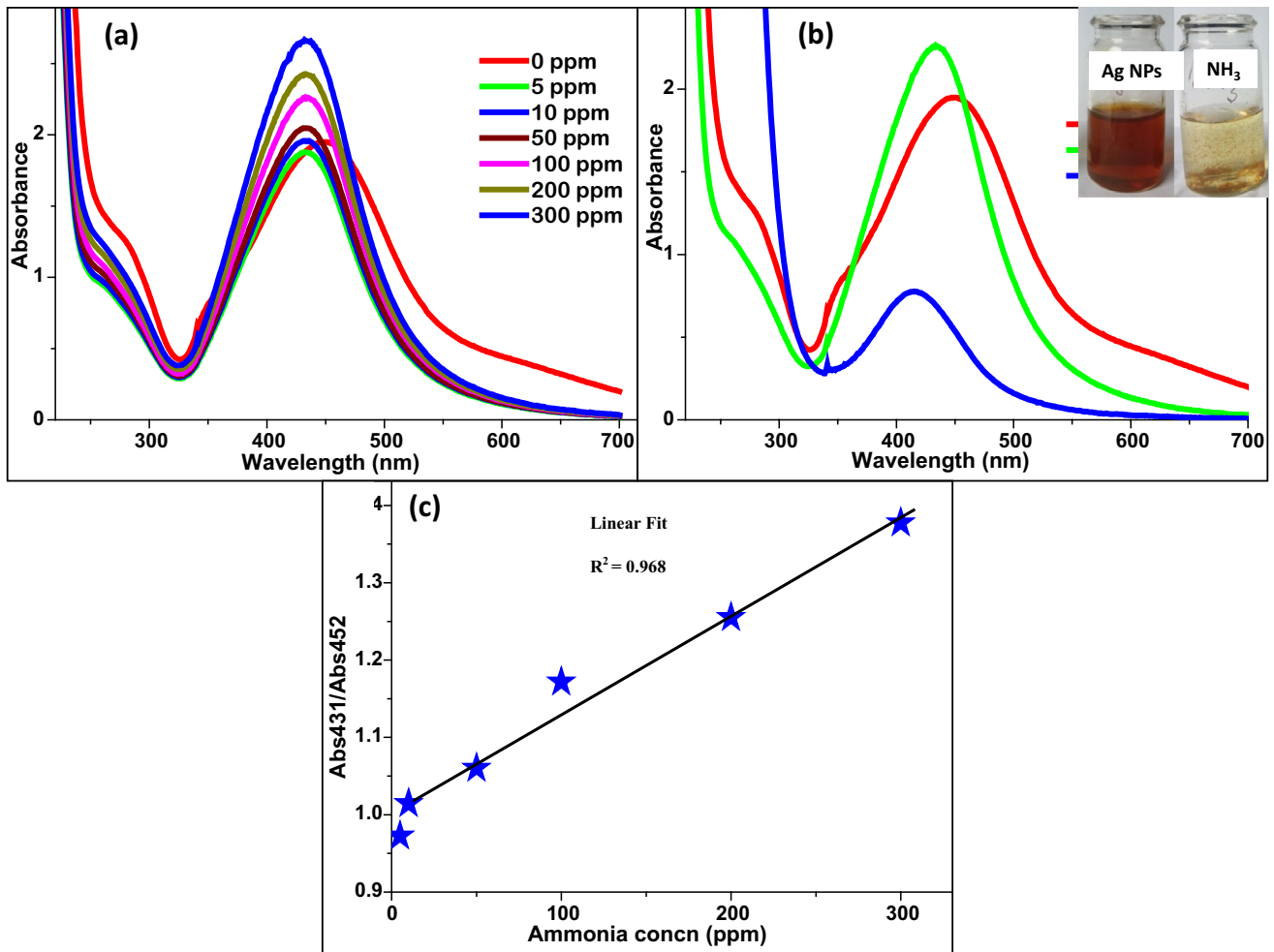
Fig. 9 a The plot of changes in UV–visible spectra of Ag NPs solution as a function of different ammonia concentration (5, 10, 50, 100, 200, and 300 ppm), **b** effect of time on color change and UV–visible spectra of Ag NPs after addition of 100 ppm ammonia solution, **c** ratio of the absorbance peaks at 429 and 452 nm is giving linear relationship as a function of different ammonia concentration (5–300 ppm) with a correlation factor $R^2 = 0.968$
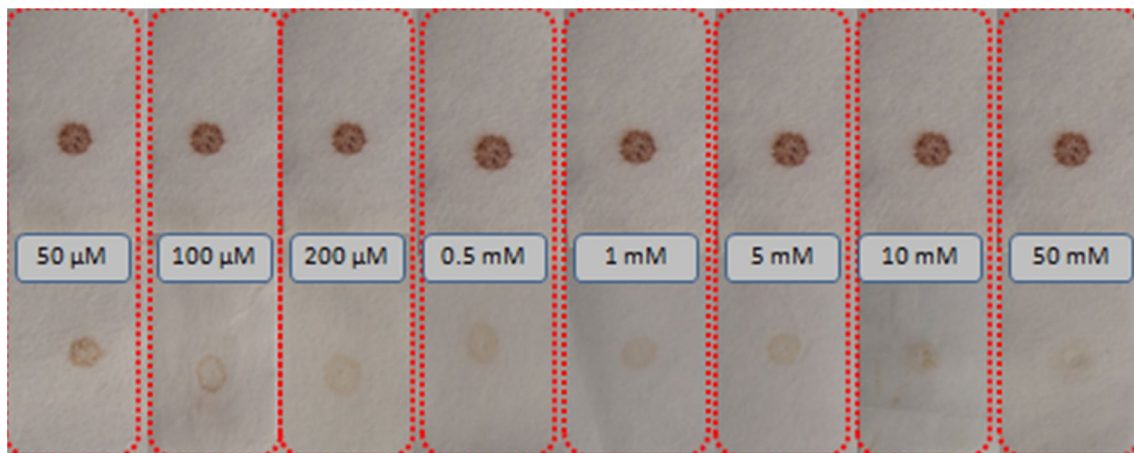

Fig. 10 Visual illustration of F-AgNPs based naked eye Hg^{II} sensor, which show change in color after treating with different concentration of mercury ions

AgNPs took more than 1 h and almost remains unchanged. Under the sub-optimal conditions, the filter paper based naked eye sensor strip could be used for the detection of mercury ion. The concentration below 50 µM could be detected, but it would take much more time. So the filter paper based Hg^{II} sensor gives a linear range from 50 µM to 50 mM as shown in Fig. 10.

Similarly Fig. 11 illustrates the images taken after the decolorization of AgNPs on filter paper after treating with aqueous ammonia. At 50 and 10 mM of ammonia solution, the AgNPs spot disappeared/decolorized after 1 min of the addition of aqueous ammonia. For 1 mM and 100 µM ammonia solution, the AgNPs spot disappeared after 5 and 8 min respectively. Similarly for 50 and 20 µM, the decolorization of AgNPs took 15 and 20 min respectively. At lower concentrations of 10 µM ammonia solution, the decolorization of AgNPs took 30 min. DI water used as positive control as shown in Fig. 11.

The phenomenon of Hg sensing using AgNPs solution was previously studies using UV–visible spectrophotometer by different investigators [54, 62–65]. At optimal experimental conditions, the prepared CF-AgNPs strip could be deployable in the field for the sensing of Hg^{II} and aqueous ammonia. Thus, at optimal conditions, CF-AgNPs naked eye sensor strip could be used for the detection of Hg^{II} and aqueous ammonia at 50 µM and 10 µM respectively within 1 h. Mercury and ammonia at further lower concentration require relatively more time for CF-AgNPs and the naked eye detection can be achieved.

3.5.4 Sensor of Cr^{VI}

Chromium toxicity largely depends on their oxidation state and it has been proved that hexavalent Cr^{VI} is more toxic than trivalent Cr^{III}. Entry of Cr^{III} into cells is very poor as compared to Cr^{VI} which can easily penetrate into cell due to their interaction with sulfate transport protein [77]. A possible metal-induced carcinogenicity of Cr^{VI} may be due to the production of hydroxyl radical. Cr^{VI} may cause different lesions of DNA such as breaks in DNA strands, sister-chromatid exchanges and sometime mutations [78, 79]. The provisional WHO guideline value for drinking-water of Cr^{VI} is 50 µg/L [70]. National primary drinking water regulations guideline value of US-EPA for chromium is 100 µg/L [71]. The possible mechanism of interaction of synthesized AgNPs with Cr^{VI} ions was studied by using UV–visible spectrophotometer. A clear change in the color of the AgNPs solution was observed after the addition of dichromate anion and exhibits a blue shift from 452 to 369 nm as shown in Fig. 12. Different concentrations of dichromate anion (5, 10, 15, 20, 25, 50, 100, 150 and 200 ppm) were used for the sensing study of AgNPs. For sensing of Cr^{VI} ions, 2 mL of AgNPs was taken in a 4 mL quartz cuvette and then added 1 mL of potassium dichromate solution and monitored their UV–visible spectra using UV–visible spectrophotometer. It was observed that after the addition of the dichromate solution to the cuvette containing AgNPs, the λ_{max} value shifted from 452 nm towards the lower wavelength with increase in intensity. Blue shift from 452 to 369 nm was observed with increasing intensity by increasing the concentration of dichromate ions from 5 to 200 ppm (Fig. 12). In the detection of dichromate anions in the solution containing multiple cations, no interference was observed during the sensing experiment from other cations. In general, the activity of ligand-functionalized sensors (chemosensor) is expensive, time consuming and sometime ligand affect the sensitivity and selectivity of sensors. Whereas, *C. cneorum* mediated AgNPs based sensor responds quickly towards the
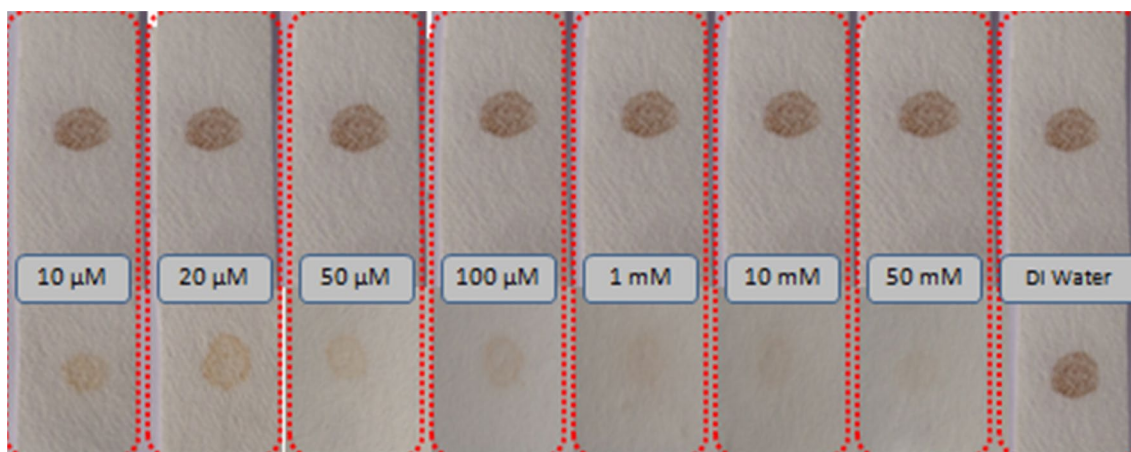

Fig. 11 Visual illustration of F-AgNPs based naked eye ammonia sensor, which show change in color after treating with different concentration of aqueous ammonia
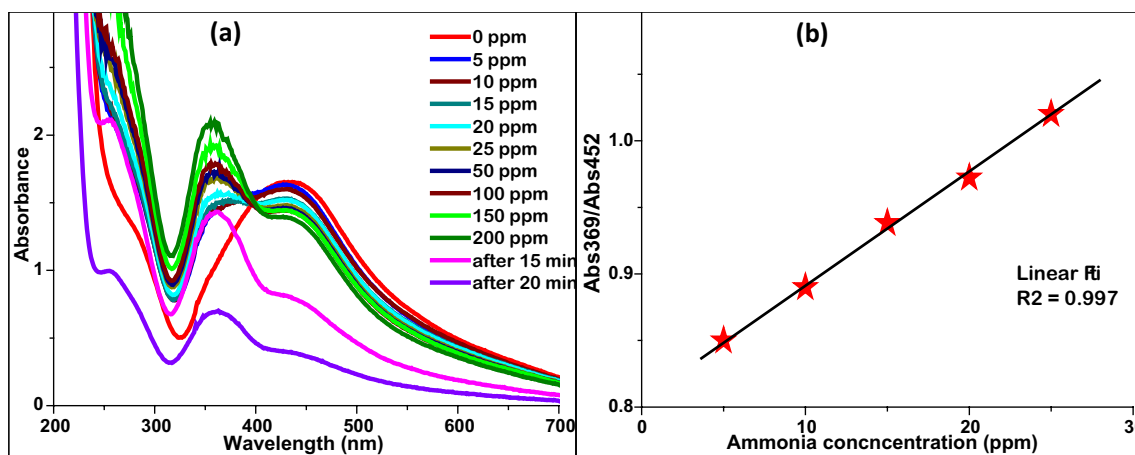
Fig. 12 **a** Plot of change in the UV–visible spectra of Ag NPs at different concentration of Cr^{VI} ions, **b** ratio of the absorbance peaks at 369 and 452 nm is giving linear relationship as a function of Cr^{VI} concentration (5–25) with a correlation factor $R^2 = 0.997$

carcinogenic Cr^{VI} ions at ambient conditions. Nontoxic, cost efficient and eco-friendly natures of our synthesized AgNPs are other important parameters over chemically synthesized AgNPs.

The selective detection of Cr^{VI} ions by our AgNPs could be explained on the bases of following possible mechanisms:

The blue shift in the λ_{max} value of AgNPs may be due to the electrochemical differences of $(Cr_2O_7)^{2-}$ anions and Ag^0. Because $(Cr_2O_7)^{2-}$ anions have $+1.33$ V standard reduction potential, whereas, the standard reduction potential of Ag is $+0.80$ V. Thus, it was also observed that the addition of Cr^{III} (-0.74) to AgNPs solution did not show any significant changes in their color or SPR. Those metals which have high reduction potentials act as an oxidizing agent.

Beside electrochemical differences, dichromate anions have a strong affinity for bonding towards the AgNPs surface and replaced the stabilizing agent of the nanoparticles and the formation of $Ag_2Cr_2O_7$. It has been previously reported [80], that the XRD pattern of $(Cr_2O_7)^{2-}$ anions treated AgNPs showed specific peaks, which are attributed to the $Ag_2Cr_2O_7$ which are, formed by the reaction of $(Cr_2O_7)^{2-}$ and Ag^+ ions.

The ratio of absorbance of the two values (abs369/abs452) is linear with dichromate concentration in the range of 5–25 ppm as shown in Fig. 12b. The correlation factor R^2 from the linear plot was found to be 0.997 as shown in Fig. 12b. The linear absorbance ratio of (abs369/abs452) showed that the AgNPs based optical sensor is active in the detection of hexavalent Cr from a range of 5–25 ppm. The shift in λ_{max} is very large and color change of AgNPs was found to take a few min. Thus, *C. cneorum* synthesized AgNPs could be used for the detection of hexavalent Cr in drinking water.

4 Conclusions

Silver NPs was synthesized successfully using aqueous leaf extract *C. cneorum*. This demonstrates natural, low-cost, fast and eco-friendly biological reducing agent for room temperature synthesis of AgNPs. The prepared nanoparticles show SPR band at 452 nm and XRD study revealed that prepared AgNPs were crystalline in nature with face centered cubic structure. EDX confirm the formation of silver colloid. The prepared AgNPs was used for optical determination of ammonia and Hg^{II}, and the SPR band show a blue shift with color change of the AgNPs solution. The nanoparticles demonstrated an excellent selectivity toward the detection of ammonia and Hg^{II} and the lower detection limit was calculated as 5 ppb for Hg^{II} determination and 5 ppm for ammonia. The desired detection limit of AgNPs is the useful limit for the detection of these toxic substances in water sample below the WHO guideline value for drinking-water. Furthermore we established the potential CF-AgNPs based sensing strip which detected the Hg^{II} and ammonia up to 5 ppm at normal condition. The current study adds additional credit for the selective, fast, eco-friendly AgNPs based nanomaterials assay for the colorimetric determination of ammonia and Hg^{II} without use of any linker or polymer with lowest detection limits in practical contaminated water samples. Filter based sensor provide us the naked eye detection of contaminants.

Compliance with ethical standards

Conflict of interest The author has no conflict of interest.

References

1. M. Moritz, M. Geszke-Moritz, The newest achievements in synthesis, immobilization and practical applications of antibacterial nanoparticles. Chem. Eng. J. **228**, 596–613 (2013)
2. M.M. Rahman, S.B. Khan, M. Faisal, A.M. Asiri, M.A. Tariq, Detection of aprepitant drug based on low-dimensional un-doped iron oxide nanoparticles prepared by a solution method. Electrochimica Acta **75**, 164–170 (2012)
3. J.L. Gardea-Torresdey, E. Gomez, J.R. Peralta-Videa, J.G. Parsons, H. Troiani, M. Jose-Yacaman, Alfalfa sprouts: a natural source for the synthesis of silver nanoparticles. Langmuir **19**, 1357–1361 (2003)
4. D. Dhanasekaran, S. Latha, S. Saha, N. Thajuddin, A. Panneerselvam, Extracellular biosynthesis, characterisation and in-vitro antibacterial potential of silver nanoparticles using *Agaricus bisporus*. J. Exp. Nanosci. **8**, 579–588 (2013)
5. M. Ismail, S. Gul, M.A. Khan, M. Khan, Plant mediated green synthesis of anti-microbial silver nanoparticles—a review on recent trends. Rev. Nanosci. Nanotechnol. **5**, 119–135 (2016)
6. S. Gul, M. Ismail, M.I. Khan, S.B. Khan, A.M. Asiri, I.U. Rahman, M.A. Khan, M.A. Kamboh, Novel synthesis of silver nanoparticles using melon aqueous extract and evaluation of their feeding deterrent activity against housefly Musca domestica. Asian Pac. J. Trop. Dis. **6**, 311–316 (2016)
7. M. Ismail, M.I. Khan, K. Akhtar, M.A. Khan, A.M. Asiri, S.B. Khan, Biosynthesis of silver nanoparticles: a colorimetric optical sensor for detection of hexavalent chromium and ammonia in aqueous solution. Phys. E: Low Dimens. Syst. Nanostruct. **103**, 367–376 (2018)
8. R.G. Munusamy, D.R. Appadurai, S. Kuppusamy, G.P. Michael, I. Savarimuthu, Ovicidal and larvicidal activities of some plant extracts against *Aedes aegypti* L. and *Culex quinquefasciatus* say (Diptera: Culicidae). Asian Pac. J. Trop. Dis. **6**, 468–471 (2016)
9. A. Rajan, V. Vilas, D. Philip, Catalytic and antioxidant properties of biogenic silver nanoparticles synthesized using *Areca catechu* nut. J. Mol. Liq. **207**, 231–236 (2015)
10. B. Ajitha, Y.A.K. Reddy, P.S. Reddy, Y. Suneetha, H.-J. Jeon, C.W. Ahn, Instant biosynthesis of silver nanoparticles using *Lawsonia inermis* leaf extract: Innate catalytic, antimicrobial and antioxidant activities. J. Mol. Liq. **219**, 474–481 (2016)
11. F. Zia, N. Ghafoor, M. Iqbal, S. Mehboob, Green synthesis and characterization of silver nanoparticles using *Cydonia oblong* seed extract. Appl. Nanosci. **6**, 1023–1029 (2016)
12. M. Bilal, S. Khan, J. Ali, M. Ismail, M.I. Khan, A.M. Asiri, S.B. Khan, Biosynthesized silver supported catalysts for disinfection of *Escherichia coli* and organic pollutant from drinking water. J. Mol. Liq. **281**, 295–306 (2019)
13. V.K. Gupta, B. Sethi, R.A. Sharma, S. Agarwal, A. Bharti, Mercury selective potentiometric sensor based on low rim functionalized thiacalix [4]-arene as a cationic receptor. J. Mol. Liq. **177**, 114–118 (2013)
14. F.M. Rebelo, E.D. Caldas, Arsenic, lead, mercury and cadmium: Toxicity, levels in breast milk and the risks for breastfed infants. Environ. Res. **151**, 671–688 (2016)
15. Q.-F. Zhang, Y.-W. Li, Z.-H. Liu, Q.-L. Chen, Reproductive toxicity of inorganic mercury exposure in adult zebrafish: histological damage, oxidative stress, and alterations of sex hormone and gene expression in the hypothalamic-pituitary-gonadal axis. Aquat. Toxicol. **177**, 417–424 (2016)
16. H.H. Harris, I.J. Pickering, G.N. George, The chemical form of mercury in fish. Science. **301**, 1203–1203 (2003)
17. M. Harada, Minamata disease: methylmercury poisoning in Japan Caused by environmental pollution. Critical Rev. Toxicol. **25**, 1–24 (1995)
18. P. Grandjean, P. Weihe, R.F. White, F. Debes, Cognitive performance of children prenatally exposed to "safe" levels of methylmercury. Environ. Res. **77**, 65–172 (1998)
19. F. Zahir, S.J. Rizwi, S.K. Haq, R.H. Khan, Low dose mercury toxicity and human health. Environ. Toxicol. Pharmacol. **20**, 351–360 (2005)
20. G.K. Darbha, A.K. Singh, U.S. Rai, E. Yu, H. Yu, P. Chandra, Ray, Selective detection of mercury (II) ion using nonlinear optical properties of gold nanoparticles. J. Am. Chem. Soc. **130**, 8038–8043 (2008)
21. M. Leermakers, W. Baeyens, P. Quevauviller, M. Horvat, Mercury in environmental samples: speciation, artifacts and validation. Trends Analyt. Chem. **24**, 383–393 (2005)
22. Y. Li, C. Chen, B. Li, J. Sun, J. Wang, Y. Gao, Y. Zhao, Z. Chai, Elimination efficiency of different reagents for the memory effect of mercury using ICP-MS. J. Analyt. At. Spectrom. **21**, 94–96 (2006)
23. Y. Wang, F. Yang, X. Yang, Colorimetric detection of mercury (II) ion using unmodified silver nanoparticles and mercury-specific oligonucleotides. ACS Appl. Mater. Inter. **2**, 339–342 (2010)
24. H.P. Borase, C.D. Patil, R.B. Salunkhe, R.K. Suryawanshi, B.K. Salunke, S.V. Patil, Mercury sensing and toxicity studies of novel latex fabricated silver nanoparticles. Bioprocess Biosyst. Eng. **37**, 2223–2233 (2014)
25. Y. Fan, Z. Liu, J. Zhan, Synthesis of starch-stabilized Ag nanoparticles and Hg^{2+} recognition in aqueous media. Nanoscale Res. Lett. **4**, 1230–1235 (2009)
26. M.M. Rahman, S.B. Khan, A. Jamal, M. Faisal, A.M. Asiri, Highly sensitive methanol chemical sensor based on undoped silver oxide nanoparticles prepared by a solution method. Microchim. Acta **178**, 99–106 (2012)
27. M. Ismail, S. Gul, M.I. Khan, M.A. Khan, A.M. Asiri, S.B. Khan, Medicago polymorpha-mediated antibacterial silver nanoparticles in the reduction of methyl orange. Green Process. Synth. **8**, 118–127 (2018)
28. R. Sriranjani, B. Srinithya, V. Vellingiri, P. Brindha, S.P. Anthony, A. Sivasubramanian, M.S. Muthuraman, Silver nanoparticle synthesis using *Clerodendrum phlomidis* leaf extract and preliminary investigation of its antioxidant and anticancer activities. J. Mol. Liq. **220**, 926–930 (2016)
29. B. Paul, B. Bhuyan, D.D. Purkayastha, S.S. Dhar, Green synthesis of silver nanoparticles using dried biomass of *Diplazium esculentum* (retz.) sw. and studies of their photocatalytic and anticoagulative activities. J. Mol. Liq. **212**, 813–817 (2015)
30. M. Umadevi, M. Bindhu, V. Sathe, A novel synthesis of malic acid capped silver nanoparticles using *Solanum lycopersicums* fruit extract. J. Mater. Sci. Technol. **29**, 317–322 (2013)
31. A. Ahmad, S. Senapati, M.I. Khan, R. Kumar, M. Sastry, Extracellular biosynthesis of monodisperse gold nanoparticles by a novel extremophilic actinomycete, *Thermomonospora* sp. Langmuir. **19**, 3550–3553 (2003)
32. S. Hamedi, S.A. Shojaosadati, A. Mohammadi, Evaluation of the catalytic, antibacterial and anti-biofilm activities of the *Convolvulus arvensis* extract functionalized silver nanoparticles. J. Photochem. Photobiol. B: Biol. **167**, 36–44 (2017)
33. S. Smitha, K. Nissamudeen, D. Philip, K. Gopchandran, Studies on surface plasmon resonance and photoluminescence of silver nanoparticles. Spectrochim. Acta A: Mol. Biomol. Spectrosc. **71**, 186–190 (2008)

34. M. Bindhu, M. Umadevi, Synthesis of monodispersed silver nanoparticles using *Hibiscus cannabinus* leaf extract and its antimicrobial activity. Spectrochim. Acta A: Mol. Biomol. Spectrosc. **101**, 184–190 (2013)

35. A. Henglein, Physicochemical properties of small metal particles in solution:" microelectrode" reactions, chemisorption, composite metal particles, and the atom-to-metal transition. J. Phys. Chem. **97**, 5457–5471 (1993)

36. J. Huang, L. Lin, Q. Li, D. Sun, Y. Wang, Y. Lu, N. He, K. Yang, X. Yang, H. Wang, Continuous-flow biosynthesis of silver nanoparticles by lixivium of sundried *Cinnamomum camphora* leaf in tubular microreactors. Ind. Eng. Chem. Res. **47**, 6081–6090 (2008)

37. S. Sandeep, A.S. Santhosh, N.K. Swamy, G.S. Suresh, J.S. Melo, P. Mallu, Biosynthesis of silver nanoparticles using *Convolvulus pluricaulis* leaf extract and assessment of their catalytic, electrocatalytic and phenol remediation properties. Adv. Mater. Lett. **7**, 383–389 (2016)

38. D. Philip, C. Unni, Extracellular biosynthesis of gold and silver nanoparticles using Krishna tulsi (*Ocimum sanctum*) leaf. Phys. E: Low Dimens. Syst. Nanostruct. **43**, 1318–1322 (2011)

39. S. Haider, T. Kamal, S.B. Khan, M. Omer, A. Haider, F.U. Khan, A.M. Asiri, Natural polymers supported copper nanoparticles for pollutants degradation. Appl. Surf. Sci. **387**, 1154–1161 (2016)

40. S.A. Khan, M. Ismail, Y. Anwar, A. Farooq, O. Al Johny Bassam, K. Akhtar, A. Shah Zafar, M. Nadeem, A. Raza Mian, A.M. Asiri, S.B. Khan, A highly efficient and multifunctional biomass supporting Ag, Ni, and Cu nanoparticles through wetness impregnation for environmental remediation. Green Process. Synth. **8**, 309–319 (2018)

41. M. Ismail, M. Khan, S.A. Khan, M. Qayum, M.A. Khan, Y. Anwar, K. Akhtar, A.M. Asiri, S.B. Khan, Green synthesis of antibacterial bimetallic Ag–Cu nanoparticles for catalytic reduction of persistent organic pollutants. J. Mater. Sci.: Mater. Electron. **29**, 20840–20855 (2018)

42. E.S. Janga, B. Sher Khan, J. Seo, H. Yoon Nama, J. Won Choia, K. Akhtard, H. Hana, Synthesis and characterization of novel UV-curable polyurethane–clay nanohybrid: influence of organically modified layered silicates on the properties of polyurethane. Prog. Org. Coatings. **71**, 36–42 (2011)

43. H. Bai, Z. Zhang, Y. Guo, G. Yang, Biosynthesis of cadmium sulfide nanoparticles by photosynthetic bacteria *Rhodopseudomonas palustris*. Colloids and Surfaces B: Biointerfaces. **70**, 142–146 (2009)

44. M. Ismail, S. Gul, M.I. Khan, M.A. Khan, A.M. Asiri, S.B. Khan, Green synthesis of zerovalent copper nanoparticles for efficient reduction of toxic azo dyes congo red and methyl orange. Green Process. Synth. **8**, 135–143 (2018)

45. N.S. Shaligram, M. Bule, R. Bhambure, R.S. Singhal, S.K. Singh, G. Szakacs, A. Pandey, Biosynthesis of silver nanoparticles using aqueous extract from the compactin producing fungal strain. Process Biochem. **44**, 939–943 (2009)

46. A.D. Dwivedi, K. Gopal, Biosynthesis of silver and gold nanoparticles using *Chenopodium album* leaf extract. Colloids Surf. A: Physicochem. Eng. Asp. **369**, 27–33 (2010)

47. N. Jain, D. Pathak, P. Mishra, S. Jain, Syntheses and antibacterial studies of some 2-[5-(Aryl)-[1, 3, 4] oxadiazole-2-ylsulfanyl] alkanoic Acids. J. Iran. Chem. Soc. **6**, 77–81 (2009)

48. Z. Ahmad Rehan, L. Gzara, S. Bahadar Khan, K.A. Alamry, M. El-Shahawi, M.H. Albeirutty, A. Figoli, E. Drioli, A.M. Asiri, Synthesis and characterization of silver nanoparticles-filled polyethersulfone membranes for antibacterial and anti-biofouling application. Recent Pat. Nanotechnol. **10**, 231–251 (2016)

49. M.M. Rahman, A. Jamal, S.B. Khan, M. Faisal, Fabrication of chloroform sensor based on hydrothermally prepared low-dimensional β-Fe_2O_3 nanoparticles. Superlattices Microstruct. **50**, 369–376 (2011)

50. B.A. Bello, S.A. Khan, J.A. Khan, F.Q. Syed, M.B. Mirza, L. Shah, S.B. Khan, Anticancer, antibacterial and pollutant degradation potential of silver nanoparticles from *Hyphaene thebaica*. Biochem. Biophys. Res. Commun. **490**, 889–894 (2017)

51. M. Ismail, M.I. Khan, S.B. Khan, M.A. Khan, K. Akhtar, A.M. Asiri, Green synthesis of plant supported CuAg and CuNi bimetallic nanoparticles in the reduction of nitrophenols and organic dyes for water treatment. J. Mol. Liq. **260**, 78–91 (2018)

52. M. Ismail, M.I. Khan, S.B. Khan, K. Akhtar, M.A. Khan, A.M. Asiri, Catalytic reduction of picric acid, nitrophenols and organic azo dyes via green synthesized plant supported Ag nanoparticles. J. Mol. Liq. **268**, 87–101 (2018)

53. T. Kamal, I. Ahmad, S.B. Khan, A.M. Asiri, Synthesis and catalytic properties of silver nanoparticles supported on porous cellulose acetate sheets and wet-spun fibers. Carbohydr. Polym. **157**, 294–302 (2017)

54. S.S. Ravi, L.R. Christena, N. SaiSubramanian, S.P. Anthony, Green synthesized silver nanoparticles for selective colorimetric sensing of Hg 2 + in aqueous solution at wide pH range. Analyst. **138**, 4370–4377 (2013)

55. P.R. Aranda, R.A. Gil, S. Moyano, I.E. De Vito, L.D. Martinez, Cloud point extraction of mercury with PONPE 7.5 prior to its determination in biological samples by ETAAS. Talanta. **75**, 307–311 (2008)

56. D.W. Boening, Ecological effects, transport, and fate of mercury: a general review. Chemosphere. **40**, 1335–1351 (2000)

57. A. Shah, T. Kazi, J. Baig, H. Afridi, G. Kandhro, M. Arain, N. Kolachi, S. Wadhwa, Total mercury determination in different tissues of broiler chicken by using cloud point extraction and cold vapor atomic absorption spectrometry. Food Chem. Toxicol. **48**, 65–69 (2010)

58. G. WHO, Guidelines for drinking-water quality. World Health Organization. **216**, 303–304 (2011)

59. B.C. Mondal, D. Das, A.K. Das, Application of a new resin functionalised with 6-mercaptopurine for mercury and silver determination in environmental samples by atomic absorption spectrometry. Anal. Chim. Acta **450**, 223–230 (2001)

60. M. Vigeh, E. Nishioka, K. Ohtani, Y. Omori, T. Matsukawa, S. Koda, K. Yokoyama, Prenatal mercury exposure and birth weight. Reproductive Toxicol. **76**, 78–83 (2018)

61. F. Kho, G.H. Pham, Absorption kinetics of mercury (II) chloride into water and aqueous sodium chloride solution. Fuel Process. Technol. **174**, 78–87 (2018)

62. P. Jarujamrus, M. Amatatongchai, A. Thima, T. Khongrangdee, C. Mongkontong, Selective colorimetric sensors based on the monitoring of an unmodified silver nanoparticles (AgNPs) reduction for a simple and rapid determination of mercury. Spectrochim. Acta A: Mol. Biomol. Spectrosc. **142**, 86–93 (2015)

63. T. Morris, H. Copeland, E. McLinden, S. Wilson, G. Szulczewski, The effects of mercury adsorption on the optical response of size-selected gold and silver nanoparticles. Langmuir. **18**, 7261–7264 (2002)

64. P. Rameshkumar, N.M. Huang, L.S. Wei, Visual and spectrophotometric determination of mercury (II) using silver nanoparticles modified with graphene oxide. Microchim. Acta **183**, 597–603 (2016)

65. P. Rameshkumar, S. Manivannan, R. Ramaraj, Silver nanoparticles deposited on amine-functionalized silica spheres and their amalgamation-based spectral and colorimetric detection of Hg (II) ions. J. Nanoparticle Res. **15**, 1639 (2013)

66. K. Roy, C.K. Sarkar, C.K. Ghosh, Rapid colorimetric detection of Hg^{2+} ion by green silver nanoparticles synthesized using *Dahlia pinnata* leaf extract. Green Process. Synth. **4**, 455–461 (2015)

67. T. Del Giacco, R. Germani, F. Purgatorio, M. Tiecco, Role of anionic micelles in self-assembling of fluorescent acridinium-based chemosensors for the detection of mercury (II) ions. J. Photochem. Photobiol. A: Chem. **345**, 74–79 (2017)

68. A.a.M. Noor, P. Rameshkumar, N.M. Huang, L.S. Wei, Visual and spectrophotometric determination of mercury(II) using silver nanoparticles modified with graphene oxide. Microchim. Acta. **183**, 597–603 (2016)

69. G.-L. Wang, X.-Y. Zhu, H.-J. Jiao, Y.-M. Dong, Z.-J. Li, Ultrasensitive and dual functional colorimetric sensors for mercury (II) ions and hydrogen peroxide based on catalytic reduction property of silver nanoparticles. Biosens. Bioelectron. **31**, 337–342 (2012)

70. W.H. Organization, Guidelines for drinking-water quality—fourth edition incorporating the first addendum (Geneva, Switzerland., 2017)

71. D.C. Rice, The US EPA reference dose for methylmercury: sources of uncertainty. Environ. Res. **95**, 406–413 (2004)

72. W. Yang, A. Zhu, J. Zhang, X. Xin, X. Zhang, Evaluation of a backward Lagrangian stochastic model for determining surface ammonia emissions. Agric. For. Meteorol. **234–235**, 196–202 (2017)

73. T. Yamada, S. Uchiyama, Y. Inaba, N. Kunugita, H. Nakagome, H. Seto, A diffusive sampling device for measurement of ammonia in air. Atmos. Environ. **54**, 629–633 (2012)

74. S.T. Dubas, V. Pimpan, Green synthesis of silver nanoparticles for ammonia sensing. Talanta. **76**, 29–33 (2008)

75. S. Pandey, G.K. Goswami, K.K. Nanda, Green synthesis of biopolymer–silver nanoparticle nanocomposite: an optical sensor for ammonia detection. Int. J. Biol. Macromol. **51**, 583–589 (2012)

76. H. Manap, M.R. Mohamed, M.S. Najib, Lower detection limit enhancement for low concentration ammonia measurement. Sens. Actuators B: Chem. **243**, 882–887 (2017)

77. K.W. Jennette, Chromate metabolism in liver microsomes. Biol. Trace Elem. Res. **1**, 55–62 (1979)

78. S. De Flora, Threshold mechanisms and site specificity in chromium (VI) carcinogenesis. Carcinogenesis. **21**, 533–541 (2000)

79. F. Depault, M. Cojocaru, F. Fortin, S. Chakrabarti, N. Lemieux, Genotoxic effects of chromium (VI) and cadmium (II) in human blood lymphocytes using the electron microscopy in situ end-labeling (EM-ISEL) assay. Toxicol. In Vitro. **20**, 513–518 (2006)

80. H. Schulz, M. Baranska, Identification and quantification of valuable plant substances by IR and Raman spectroscopy. Vib. Spectrosc. **43**, 13–25 (2007)

Publisher's Note Springer Nature remains neutral with regard to jurisdictional claims in published maps and institutional affiliations.